

Research Paper

# Free Damped Vibration Analysis of Sandwich Plates with CNT-Reinforced MRE Core and Laminated Three-Phase Polymer/GPL/Fiber Face Sheets

A. Karbasizadeh<sup>1</sup>, A. Ghorbanpour Arani<sup>1,2\*</sup>, S. Niknejad<sup>1</sup>, Z. Khoddami Maraghi<sup>3</sup>

<sup>1</sup> Faculty of Mechanical Engineering, University of Kashan, Kashan, Iran P.O. Box 87317-53153

<sup>2</sup> Institute of Nanoscience & Nanotechnology, University of Kashan, Kashan, Iran

<sup>3</sup> Faculty of Engineering, Mahallat Institute of Higher Education, Mahallat, Iran

Received 19 September 2022; Received in revised form 6 February 2023; Accepted 6 December 2023

## ABSTRACT

In this article, an analytical solution is provided for the free damped vibration analysis of a sandwich plate resting on a visco-Pasternak foundation. The plate consists of a magnetorheological elastomer (MRE) core reinforced with carbon nanotubes (CNTs) and laminated polymer-based face sheets enriched with graphene nanoplatelets (GPLs) and glass fibers. The governing equations and associated boundary conditions are derived utilizing Hamilton's principle and are solved analytically using Navier's method for a simply supported plate. The influences of various parameters on the natural frequencies and corresponding loss factors are examined such as aspect ratio of the plate, thickness-to-length of the plate, magnetic field intensity, thickness of the MRE core, mass fraction of the CNTs in the MRE core, mass fractions of the GPLs and fibers in the face sheets, and Winkler, Pasternak, and damping coefficients of the foundation. It is shown that adjoining CNTs to the MRE core leads to a small increase in the natural frequencies and loss factors of the plate. Consequently, due to the high cost of the CNTs, adding them to the MRE core to improve the vibrational characteristics of the sandwich plates with MRE core is not an optimum design.

**Keywords:** Vibration; Magnetorheological materials; Carbon nanotubes; Graphene nanoplatelets.

\*Corresponding author. Tel.: +98 31 55912450, Fax: +98 31 55912424.

E-mail address: aghorban@kashanu.ac.ir

## 1 INTRODUCTION

**D**UE to the advantages and disadvantages of materials, a single-layer structure is not an optimum design. To benefit from the advantages and reduce the side effects of the disadvantages, sandwich and multi-layered structures can be utilized [1-4]. The material selected for face sheets of a sandwich structure should benefit from high stiffness and the material utilized as the core should benefit from low density. One of the popular materials which can be utilized as the core in sandwich structures is magnetorheological materials (MRs). MRs such as magnetorheological fluids (MRF) and magnetorheological elastomers (MRE) are kinds of materials with controllable rheology. The MRs contain suspended micro-sized particles which are sensitive to applied magnetic fields. When an MR material is exposed to a magnetic field, the arrangement of the particles varies in a uniform way which affects the mechanical properties of the materials in a restorable way. There is a wide range of works associated with the vibration analysis of sandwich structures with MRE or MRF cores.

An experimental study was presented by Lara-Prieto et al. [5] to analyze the free vibration of cantilever sandwich beams with MR core. The tunability of the stiffness and damping characteristics of the beams with the MR core was confirmed by them. The dynamic buckling behavior of three-layered sandwich beams with conductive skins and partially MRE core was investigated by Nayak et al. [6]. It was shown by them that the higher percentage of iron particles and higher magnetic field result in better stability of the structure. In a similar work, they studied the dynamic buckling analysis of spinning three-layered sandwich beams with conductive skins and an MRE core. They focused on the effects of the magnetic field intensity and rotational speed on the stability regions [7]. Rajamohan et al. [8] employed the finite element method (FEM) and presented a numerical solution for the free vibration analysis of sandwich beams with MRF core. It was observed by them that the higher magnetic field intensity results in higher natural frequencies and loss factors. Navazi et al. [9] studied the free vibration analysis of doubly tapered sandwich beams with MRE core. They confirmed that there is an optimum value of the magnetic field which results in the highest loss factor of the beam. The effects of magnetoelastic loads on the free vibrational characteristics of the MR-based sandwich beams were investigated by Rokn-Abadi et al. [10]. It was observed by them that the effects of the magnetoelastic loads are more obvious with the higher beam length. Omid Soroor et al. [11] studied the free vibrational analysis of sandwich beams consisting of a homogenous isotropic base layer, an MRF core, and an axially functionally graded (FG) constraining layer. They revealed that by increasing the thickness of the MRF core the natural frequencies diminish and the loss factors experience an initial steep reduction, followed by moderate growth. Aguib et al. [12] presented numerical and experimental results for the vibrational characteristics of sandwich plates with an MRE core. It was observed by them that the higher magnetic field intensity results in a lower resonance amplitude. The free vibrational behavior of multi-layered sandwich plates with a flexible core and MRF layers embedded between composite sheets was investigated by Payganeh et al. [13]. They concluded that to enhance the natural frequencies, it is more useful to utilize thinner MRF layers. Yeh [14] studied the free vibrational characteristics of orthotropic rectangular sandwich thin plates with isotropic homogenous face sheets and an MRE core. He found that the natural frequencies grow with an increase in the magnetic field intensity. Eshaghi [15] investigated the effects of MRF core on the aeroelastic stability characteristics of sandwich plates with MRF core. It was concluded by him that the higher magnetic field intensity results in better aeroelastic stability.

Due to high values of elastic moduli and low density, CNTs have been extensively utilized as the reinforcement in the structures. Many authors have focused on the positive effects of CNTs on the mechanical characteristics of the structures [16-21]. Recently, Selvaraj and his co-workers presented some works regarding the mechanical characteristics of sandwich structures with CNT-reinforced MR core [22-26]. Selvaraj and Ramamoorthy [22] presented experimental and numerical analyses on the free vibration of sandwich beams with CNT-reinforced MRE core. They concluded that the presence of CNTs improves the free vibration characteristics of MRE. In another work, they focused on the dynamic characteristics of laminated composite sandwich beams with CNT-reinforced MRE core [23]. They concluded that the presence of CNTs in MREs not only creates a higher stiffness of the beam but also enhances its damping characteristics. Dynamic characteristics of laminated composite cylindrical sandwich shells with CNT-reinforced MRE core were investigated by Arumugam et al. [24]. It was demonstrated by them that the natural frequencies of such structures decrease by increasing the CNT-MRE thickness. Numerical and experimental results were provided by Selvaraj et al. [25] on the free vibration characteristics of rotating composite sandwich beams with CNT-reinforced MRE core. They concluded that higher percentages of the CNTs in the MRE core result in higher natural frequencies and loss factors. Selvaraj et al. [26] studied the free and forced vibration characteristics of sandwich beams with laminated composite face sheets and a partially configured CNT-reinforced MRE core. They employed the genetic algorithm (GA) to find the optimal positions of the MRE core to maximize the natural frequencies and loss factors.

In the presented article, the free damped vibrational characteristics of sandwich rectangular plates with a CNT-reinforced MRE core and laminated three-phase polymer/GPL/fiber face sheets resting on a visco-Pasternak foundation were investigated for the first time. The effects of various parameters on the natural frequencies and loss factors are investigated including geometrical parameters of the plate, the thickness of the MRE core, magnetic field intensity, mass fraction of the CNTs in the MRE core, and mass fractions of the GPLs and fibers in the face sheets. As the novelty of the presented work, it can be stated that there are lots of works regarding the free vibration analysis of the sandwich plates with MR core and isotropic homogenous face sheets. But the presented work is the first work that investigates the vibrational characteristics of a sandwich plate with a CNT-reinforced MRE core and laminated three-phase polymer/GPL/fiber face sheets.

## 2 MATHEMATICAL MODELING

As depicted in Fig. 1, a sandwich rectangular plate of length  $b$  and width  $a$  resting on a visco-Pasternak foundation is considered. The face sheets are laminated three-phase polymer/GPL/fiber face sheets and the core is made of a CNT-reinforced MRE. The thickness of the bottom, core, and top layers sequentially are shown by  $h_1, h_2, h_3$ .

It is assumed that the MRE core does not bear considerable normal stress and it can only bear the shear components of the stress tensor which can be presented as follows [14]:

$$\sigma_{xz}^{(2)} = G_2^* \gamma_{xz}^{(2)}, \quad \sigma_{yz}^{(2)} = G_2^* \gamma_{yz}^{(2)}, \quad (1)$$

where  $\gamma_{xz}^{(2)}$  and  $\gamma_{yz}^{(2)}$  are shear components of the stress tensor at the MRE core and with the following definition,

$$G_2^* \text{ is a complex value known as the complex shear modulus of MRE [14]:} \\ G_2^* = G_0 (1 + i\eta_0) \quad (2)$$

in which  $i^2 = -1$  and  $G_0$  and  $\eta_0$  are known as the storage modulus and loss factor. These parameters can be found in Table 1 for an MRE reinforced with multi-walled carbon nanotubes (MWCNTs) with various values of mass fraction of the CNTs ( $W_{CNT}$ ) and magnetic field intensity ( $B$ ). These experimental values are provided by Selvaraj et al. [25].

In this paper, the third-order polynomials provided in Eq. (3.a) are utilized to estimate the values provided in Table 1. It is noteworthy that second-order polynomials presented in Eq. (3.b) are recommended by Selvaraj et al. [25]. As shown in Fig. 2, the polynomials recommended by Selvaraj et al. [25] are not accurate enough for estimating loss factors.

$$\left\{ \begin{array}{l} W_{CNT} = 0 : \\ G_0(Pa) = 0.001259B^3 - 0.888B^2 + 771.3B + 636000, \\ \eta_0 = (5.397 \times 10^{-10})B^3 - (5.064 \times 10^{-7})B^2 + (1.557 \times 10^{-4})B + 0.0912, \\ W_{CNT} = 0.005 \text{ (0.5\%)} : \\ G_0(Pa) = -0.001344B^3 + 0.6B^2 + 586B + 811000, \\ \eta_0 = (-2.347 \times 10^{-11})B^3 - (4.24 \times 10^{-8})B^2 + (8.167 \times 10^{-5})B + 0.0926, \\ W_{CNT} = 0.01 \text{ (1\%)} : \\ G_0(Pa) = 0.000128B^3 - 0.528B^2 + 816B + 868000 \\ \eta_0 = (2.304 \times 10^{-10})B^3 - (2.752 \times 10^{-7})B^2 + (1.34 \times 10^{-4})B + 0.0991. \end{array} \right. \quad (3.a)$$

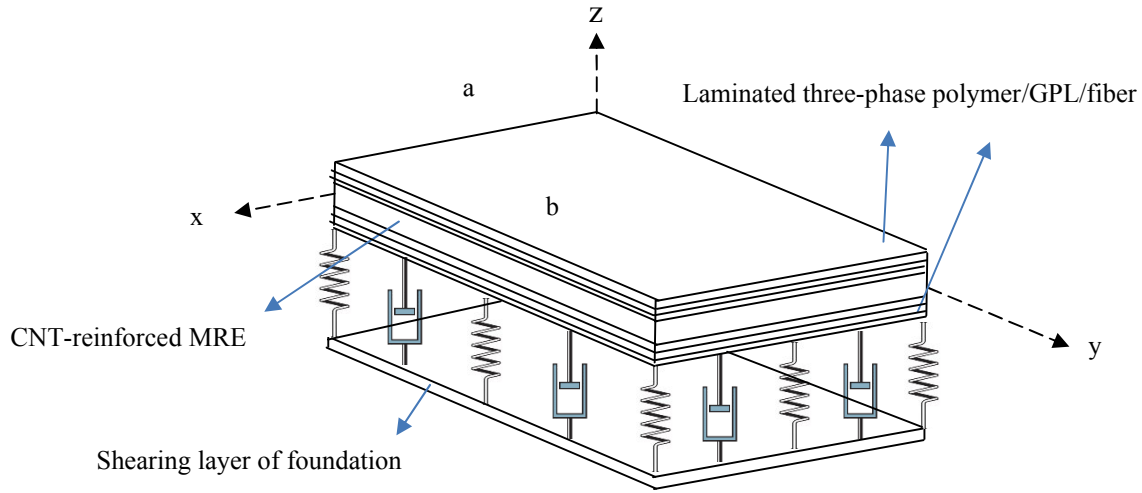


**Fig. 1**  
Schematic of the problem.

$$\left\{ \begin{array}{l}
 W_{CNT} = 0 : \\
 G_0 (Pa) = -0.0241B^2 + 644.67B + 639600, \\
 \eta_0 = -10^{-7} B^2 + 10^{-4} B + 0.0919, \\
 W_{CNT} = 0.005 \text{ (0.5\%)} : \\
 G_0 (Pa) = -0.3588B^2 + 732.3B + 810100, \\
 \eta_0 = -(6 \times 10^{-8}) B^2 + (8 \times 10^{-5}) B + 0.0926, \\
 W_{CNT} = 0.01 \text{ (1\%)} : \\
 G_0 (Pa) = -0.5489B^2 + 833.01B + 868100 \\
 \eta_0 = -(3 \times 10^{-8}) B^2 + (4 \times 10^{-5}) B + 0.0995.
 \end{array} \right. \quad (3.b)$$

**Table 1**  
Storage modulus and loss factor of CNT-reinforced MRE [25]

| $B$ (Gauss) | $W_{CNT}=0$           |             | $W_{CNT}=0.005$ (0.5 %) |             | $W_{CNT}=0.01$ (1 %)  |             |
|-------------|-----------------------|-------------|-------------------------|-------------|-----------------------|-------------|
|             | Storage modulus (MPa) | Loss factor | Storage modulus (MPa)   | Loss factor | Storage modulus (MPa) | Loss factor |
| 0           | 0.636                 | 0.0912      | 0.811                   | 0.0926      | 0.868                 | 0.0991      |
| 125         | 0.721                 | 0.1038      | 0.891                   | 0.1021      | 0.962                 | 0.1120      |
| 250         | 0.793                 | 0.1069      | 0.974                   | 0.1100      | 1.041                 | 0.1190      |
| 500         | 0.957                 | 0.1099      | 1.086                   | 0.1199      | 1.160                 | 0.1261      |

The variations of storage modulus and loss factor versus the variation of magnetic field intensity are depicted in Fig. 2 for various values of mass fraction of the CNTs. This figure reveals that as the mass fraction of the CNTs grows, the storage modulus increases for all values of magnetic field intensity, and the loss factor increases for most values of magnetic field intensity.

An MRE contains suspended micro-sized particles (Fig. 3.a) which are sensitive to an applied magnetic field. When an MRE is exposed to a magnetic field, the arrangement of the particles varies in a uniform way which affects the mechanical properties of the materials in a restorable way (Fig. 3.b). As the magnetic field intensity grows, more micro-sized particles are affected which results in higher shear modulus which can be seen in Fig. 2. Fig. 2 also shows that an increase in the mass fraction of the CNTs leads to higher storage modulus which can be explained by high values of the elastic moduli of the CNTs.

### 2.1. Effective mechanical properties

Due to the high cost of CNTs and GPLs and also their agglomeration when used in high percentages, three-phase composite materials have attracted high attention of researchers in recent years [27-29]. A three-phase composite polymer/GPL/fiber consists of a polymeric matrix enriched with GPLs and reinforced with micro-scaled fibers such as glass, boron fibers, or aramid. Here the subscripts  $m$ ,  $GPL$ ,  $f$ , and  $gm$  are utilized to show the properties of the matrix, GPLs, fibers, and GPL-reinforced matrix, respectively. It should be noted that in some cases, superscript  $f$  is employed to show the properties of fibers.

According to the rule of mixture, the density ( $\rho$ ) and Poisson's ratio ( $\nu$ ) of the GPL-reinforced matrix can be stated in terms of their volume fraction ( $V$ ) as follows [30, 31]:

$$\rho_{gm} = \rho_{GPL}V_{GPL} + \rho_m V_m, \quad \nu_{gm} = \nu_{GPL}V_{GPL} + \nu_m V_m, \quad (4)$$

For the GPLs, the volume fraction can be presented as follows [32]:

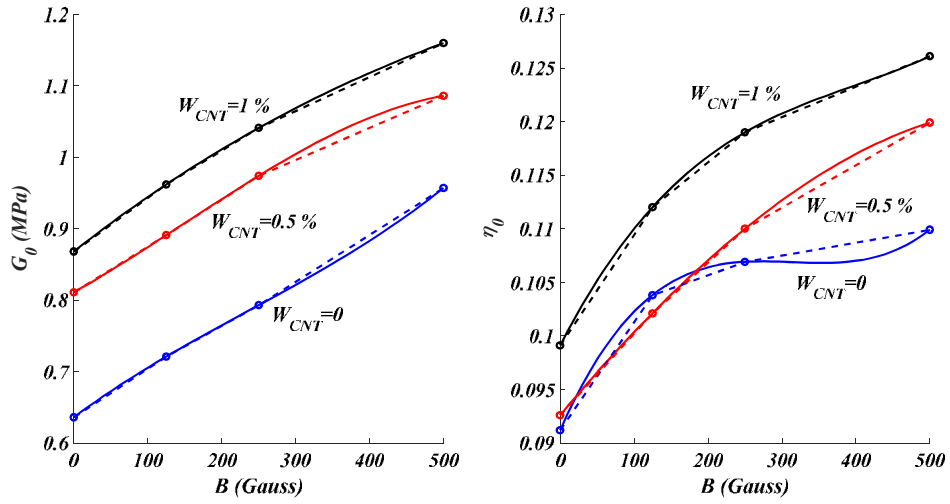
$$V_{GPL} = \frac{1}{1 + \frac{\rho_{GPL}}{\rho_m} \left( \frac{1}{W_{GPL}} - 1 \right)}, \quad (5)$$

in which  $W_{GPL}$  indicates the weight fraction of the GPLs. For the matrix, the volume fraction can be calculated as

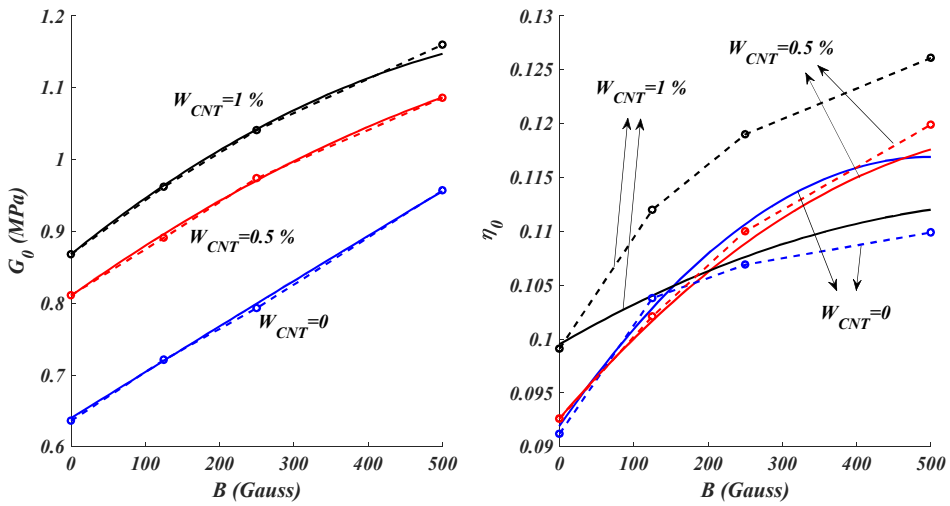
$$V_m = 1 - V_{GPL}. \quad (6)$$

Based on the Halpin-Tsai model, the effective modulus of elasticity ( $E$ ) of the GPL-reinforced polymeric matrix can be stated as follows [33]:

$$E_{gm} = \frac{1}{8} \left[ \frac{3(1 + \xi_L \eta_L V_{GPL})}{1 - \eta_L V_{GPL}} + \frac{5(1 + \xi_w \eta_w V_{GPL})}{1 - \eta_w V_{GPL}} \right] E_m, \quad (7)$$



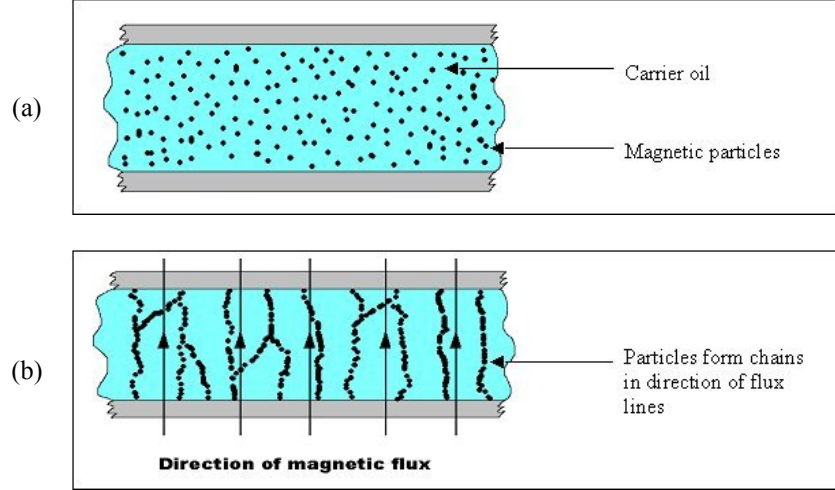
(a) Present work: (-) Third-order polynomials, (--o) Experimental data



(b) Selvaraj et al. [25]: (-) Second-order polynomials, (--o) Experimental data

**Fig. 2**

Accuracy of the polynomials provided for the data presented in Table 1, (a) Present work, (b) Selvaraj et al. [25].

**Fig. 3**

The effect of magnetic field on an MRE elastomer.

where

$$\xi_L = \frac{2l_{GPL}}{h_{GPL}}, \quad \xi_w = \frac{2w_{GPL}}{h_{GPL}}, \quad \eta_L = \frac{\eta - 1}{\eta + \xi_L}, \quad \eta_w = \frac{\eta - 1}{\eta + \xi_w}, \quad \eta = \frac{E_{GPL}}{E_m}, \quad (8)$$

in which  $l_{GPL}$ ,  $w_{GPL}$ , and  $h_{GPL}$  respectively stand for the length, width, and thickness of the GPLs. As the GPL-reinforced matrix is an isotropic material, its shear modulus can be stated as follows:

$$G_{gm} = \frac{E_{gm}}{2(1 + \nu_{gm})}. \quad (9)$$

Based on the rule of mixture, the density of the three-phase material can be stated as [34, 35]

$$\rho = \rho_f V_f + \rho_{gm} V_{gm}, \quad (10)$$

where the following relation can be utilized to calculate the volume fraction of the fibers [34, 35]:

$$V_f = \frac{1}{1 + \frac{\rho_f}{\rho_{gm}} \left( \frac{1}{W_f} - 1 \right)}. \quad (11)$$

in which  $W_f$  is the weight fraction of the fibers. The volume fraction of the GPL-reinforced polymeric matrix can be stated as follows:

$$V_{gm} = 1 - V_f. \quad (12)$$

For the three-phase material, the elastic and shear moduli and Poisson ratios can be calculated utilizing the following micromechanical relations ( $\nu_{21} = \nu_{12} E_{22} / E_{11}$ ) [34, 35]:

$$\begin{aligned}
 E_{11} &= E_{11}^f V_f + E_{gm} V_{gm}, & E_{22} &= \frac{E_{22}^f + E_{gm} + (E_{22}^f - E_{gm}) V_f}{E_{22}^f + E_{gm} - (E_{22}^f - E_{gm}) V_f} E_{gm}, \\
 \nu_{12} &= \nu_{12}^f V_f + \nu_{gm} V_{gm}, & G_{12} &= \frac{G_{12}^f + G_{gm} + (G_{12}^f - G_{gm}) V_f}{G_{12}^f + G_{gm} - (G_{12}^f - G_{gm}) V_f} G_{gm}.
 \end{aligned} \tag{13}$$

## 2.2. Equations of motion

The plate consists of a moderately thick core and two thin face sheets. Consequently, the face sheets can be modeled based on the classical plate theory (CPT) and the MRE core can be modeled based on the first-order shear deformation theory (FSDT). Based on the CPT, the displacement field in the thin face sheets ( $k=1,3$ ) can be described as follows [14]:

$$\begin{aligned}
 \hat{u}_k(x, y, z, t) &= u_k(x, y, t) - z_k \frac{\partial w}{\partial x}, \\
 \hat{v}_k(x, y, z, t) &= v_k(x, y, t) - z_k \frac{\partial w}{\partial y}, \\
 \hat{w}_k(x, y, z, t) &= w(x, y, t),
 \end{aligned} \tag{14}$$

in which  $\hat{u}_k$ ,  $\hat{v}_k$  and  $\hat{w}_k$  respectively indicate the displacement in the  $k$ th layer in  $x$ ,  $y$ , and  $z$  directions, and  $u_k$ ,  $v_k$  and  $w$  stand for the corresponding displacement at the middle surface of each layer ( $z_k=0$ ). Based on the FSDT, the displacement field in the core (specified with the subscript  $c$ ) can be considered as

$$\begin{aligned}
 \hat{u}_2(x, y, z, t) &= u_2(x, y, t) + z_2 \alpha_2(x, y, t), \\
 \hat{v}_2(x, y, z, t) &= v_2(x, y, t) + z_2 \beta_2(x, y, t), \\
 \hat{w}_2(x, y, z, t) &= w(x, y, t),
 \end{aligned} \tag{15}$$

where  $\alpha_2$  and  $\beta_2$  are the rotation about  $y$ - and  $x$ -axes, sequentially.

The continuity of displacement between three layers of the plate can be stated as follows:

$$\hat{u}_2\left(x, y, -\frac{h_2}{2}, t\right) = \hat{u}_1\left(x, y, \frac{h_1}{2}, t\right), \quad \hat{u}_2\left(x, y, \frac{h_2}{2}, t\right) = \hat{u}_3\left(x, y, -\frac{h_3}{2}, t\right). \tag{16}$$

Utilizing Eqs. (14)-(16) and considering the same thickness for the face sheets ( $h_1=h_3=h_f$ ), the following relation can be obtained:

$$u_2 = \frac{u_1 + u_3}{2}, \quad v_2 = \frac{v_1 + v_3}{2}, \quad \alpha_2 = \frac{u_3 - u_1}{h_2} + \frac{h_f}{h_2} \frac{\partial w}{\partial x}, \quad \beta_2 = \frac{v_3 - v_1}{h_2} + \frac{h_f}{h_2} \frac{\partial w}{\partial y}. \tag{17}$$

By substituting Eq. (17) into Eq. (16), the displacement field in the MRE core can be described as follows:

$$\hat{u}_2 = \frac{u_1 + u_3}{2} + \frac{z_2}{h_2} \left( u_3 - u_1 + h_f \frac{\partial w}{\partial x} \right), \quad \hat{v}_2 = \frac{v_1 + v_3}{2} + \frac{z_2}{h_2} \left( v_3 - v_1 + h_f \frac{\partial w}{\partial y} \right), \quad \hat{w}_2 = w. \tag{18}$$

The normal ( $\varepsilon_{ij}$ ) and shear ( $\gamma_{ij}$ ) components of the strain tensor in the face sheets can be stated as follows:

$$\begin{aligned}\varepsilon_{xx}^{(k)} &= \frac{\partial \hat{u}_k}{\partial x} = \frac{\partial u_k}{\partial x} - z_k \frac{\partial^2 w}{\partial x^2}, & \varepsilon_{yy}^{(k)} &= \frac{\partial \hat{v}_k}{\partial y} = \frac{\partial v_k}{\partial y} - z_k \frac{\partial^2 w}{\partial y^2}, \\ \gamma_{xy}^{(k)} &= \frac{\partial \hat{u}_k}{\partial y} + \frac{\partial \hat{v}_k}{\partial x} = \frac{\partial u_k}{\partial y} + \frac{\partial v_k}{\partial x} - 2z_k \frac{\partial^2 w}{\partial x \partial y},\end{aligned}\quad (19)$$

and for the MRE core, the following equation can be stated for the shear components of strain:

$$\gamma_{xz}^{(2)} = \frac{\partial \hat{u}_2}{\partial z_2} + \frac{\partial \hat{w}_2}{\partial x} = \frac{u_3 - u_1}{h_2} + d \frac{\partial w}{\partial x}, \quad \gamma_{yz}^{(2)} = \frac{\partial \hat{v}_2}{\partial z_2} + \frac{\partial \hat{w}_2}{\partial y} = \frac{v_3 - v_1}{h_2} + d \frac{\partial w}{\partial y}, \quad (20)$$

in which

$$d = 1 + \frac{h_f}{h_2}. \quad (21)$$

The components of the stress tensor in the face sheets can be obtained as

$$\begin{Bmatrix} \sigma_{xx}^{(k)} \\ \sigma_{yy}^{(k)} \\ \sigma_{xy}^{(k)} \end{Bmatrix} = \begin{bmatrix} Q_{11}^{(k)} & Q_{12}^{(k)} & 0 \\ Q_{12}^{(k)} & Q_{22}^{(k)} & 0 \\ 0 & 0 & Q_{66}^{(k)} \end{bmatrix} \begin{Bmatrix} \varepsilon_{xx}^{(k)} \\ \varepsilon_{yy}^{(k)} \\ \gamma_{xy}^{(k)} \end{Bmatrix}, \quad (22)$$

where

$$Q_{11}^{(k)} = \frac{E_{11}^{(k)}}{1 - \nu_{12}^{(k)} \nu_{21}^{(k)}}, \quad Q_{22}^{(k)} = \frac{E_{22}^{(k)}}{1 - \nu_{12}^{(k)} \nu_{21}^{(k)}}, \quad Q_{12}^{(k)} = \nu_{12}^{(k)} Q_{22}^{(k)}, \quad Q_{66}^{(k)} = G_{12}^{(k)}. \quad (23)$$

Based on Hamilton's principle, by considering  $\delta$  as the variational operator and  $[t_1, t_2]$  as an arbitrary time interval, the set of the governing equations and associated boundary conditions can be derived using the following relation [36]:

$$\int_{t_1}^{t_2} (\delta T - \delta U_s + \delta W_{n.c.}) dt = 0, \quad (24)$$

where  $T$  and  $U_s$  sequentially stand for the kinetic energy and strain energy, and  $W_{n.c.}$  is the work done by the external non-conservative loads.

The kinetic energy of the plate can be presented as follows:

$$T = \sum_{k=1}^3 \frac{1}{2} \iiint_{V_k} \rho \left[ \left( \frac{\partial \hat{u}_k}{\partial t} \right)^2 + \left( \frac{\partial \hat{v}_k}{\partial t} \right)^2 + \left( \frac{\partial \hat{w}_k}{\partial t} \right)^2 \right] dV_k, \quad (25)$$

where  $V_k$  is the volume of the  $k$ th layer:

$$\iiint_{V_k} ( ) dV_k = \iint_S \int_{-\frac{h_k}{2}}^{\frac{h_k}{2}} ( ) dz_k dS. \quad (26)$$

in which  $S$  stands for the surface of the plate.

The densities of the core and the face sheets do not change through the thickness direction; Consequently, one can write

$$\int_{-\frac{h_1}{2}}^{\frac{h_1}{2}} \rho_1 z_1 dz_1 = \int_{-\frac{h_2}{2}}^{\frac{h_2}{2}} \rho_2 z_2 dz_2 = \int_{-\frac{h_3}{2}}^{\frac{h_3}{2}} \rho_3 z_3 dz_3 = 0, \quad (27)$$

and Eq. (25) can be presented as

$$T = \frac{1}{2} \iint_S \left\{ I_0 \left( \frac{\partial w}{\partial t} \right)^2 + I_0^{(1)} \left[ \left( \frac{\partial u_1}{\partial t} \right)^2 + \left( \frac{\partial v_1}{\partial t} \right)^2 \right] + I_0^{(3)} \left[ \left( \frac{\partial u_3}{\partial t} \right)^2 + \left( \frac{\partial v_3}{\partial t} \right)^2 \right] \right. \\ \left. + \left( I_2^{(1)} + I_2^{(3)} \right) \left[ \left( \frac{\partial^2 w}{\partial t \partial x} \right)^2 + \left( \frac{\partial^2 w}{\partial t \partial y} \right)^2 \right] + I_0^{(2)} \left[ \left( \frac{\partial u_2}{\partial t} \right)^2 + \left( \frac{\partial v_2}{\partial t} \right)^2 \right] + I_2^{(2)} \left[ \left( \frac{\partial \alpha_2}{\partial t} \right)^2 + \left( \frac{\partial \beta_2}{\partial t} \right)^2 \right] \right\} dS, \quad (28)$$

in which the inertia terms are defined as follows:

$$I_0^{(k)} = \int_{-\frac{h_k}{2}}^{\frac{h_k}{2}} \rho_k dz_k, \quad I_2^{(k)} = \int_{-\frac{h_k}{2}}^{\frac{h_k}{2}} \rho_k z_k^2 dz_k, \quad I_0 = I_0^{(1)} + I_0^{(2)} + I_0^{(3)}. \quad (29)$$

The strain energy of the plate can be presented stated as

$$U_s = \sum_{k=1}^3 \frac{1}{2} \iiint_{V_k} \sigma_{ij}^{(k)} \varepsilon_{ij}^{(k)} dV_k, \quad (30)$$

and the variation of the strain energy of the plate can be found as follows:

$$\delta U_s = \sum_{k=1}^3 \iiint_{V_k} \sigma_{ij}^{(k)} \delta \varepsilon_{ij}^{(k)} dV_k. \quad (31)$$

Eq. (31) can be represented in the following expanded form:

$$\delta U_s = \sum_{k=1,3} \iiint_{V_k} \left( \sigma_{xx}^{(k)} \delta \varepsilon_{xx}^{(k)} + \sigma_{yy}^{(k)} \delta \varepsilon_{yy}^{(k)} + \sigma_{xy}^{(k)} \delta \gamma_{xy}^{(k)} \right) dV_k + \iiint_{V_2} \left( \sigma_{xz}^{(2)} \delta \gamma_{xz}^{(2)} + \sigma_{yz}^{(2)} \delta \gamma_{yz}^{(2)} \right) dV_2, \quad (32)$$

which can be rewritten utilizing Eqs. (19), (20), and (26) as

$$\delta U_s = \iint_S \left( N_{xx}^{(1)} \frac{\partial \delta u_1}{\partial x} - M_{xx} \frac{\partial^2 \delta w}{\partial x^2} + N_{yy}^{(1)} \frac{\partial \delta v_1}{\partial y} - M_{yy} \frac{\partial^2 \delta w}{\partial y^2} + N_{xy}^{(1)} \frac{\partial \delta u_1}{\partial y} \right. \\ \left. + N_{xy}^{(1)} \frac{\partial \delta v_1}{\partial x} - 2M_{xy} \frac{\partial^2 \delta w}{\partial x \partial y} + N_{xx}^{(3)} \frac{\partial \delta u_3}{\partial x} + N_{yy}^{(3)} \frac{\partial \delta v_3}{\partial y} + N_{xy}^{(3)} \frac{\partial \delta u_3}{\partial y} + N_{xy}^{(3)} \frac{\partial \delta v_3}{\partial x} \right. \\ \left. + \frac{Q_{xz}^{(2)}}{h_2} \delta u_3 - \frac{Q_{xz}^{(2)}}{h_2} \delta u_1 + Q_{xz}^{(2)} d \frac{\partial \delta w}{\partial x} + \frac{Q_{yz}^{(2)}}{h_2} \delta v_3 - \frac{Q_{yz}^{(2)}}{h_2} \delta v_1 + Q_{yz}^{(2)} d \frac{\partial \delta w}{\partial y} \right) dS, \quad (33)$$

where the stress resultants are defined as follows:

$$\left\{ \begin{matrix} N_{ij}^{(k)} \\ M_{ij}^{(k)} \end{matrix} \right\} = \int_{-\frac{h_k}{2}}^{\frac{h_k}{2}} \sigma_{ij}^{(k)} \left\{ \begin{matrix} 1 \\ z_k \end{matrix} \right\} dz_k, \quad \left\{ \begin{matrix} Q_{xz}^{(2)} \\ Q_{yz}^{(2)} \end{matrix} \right\} = \int_{-\frac{h_2}{2}}^{\frac{h_2}{2}} \left\{ \begin{matrix} \sigma_{xz}^{(2)} \\ \sigma_{yz}^{(2)} \end{matrix} \right\} dz_2, \quad (34)$$

$$M_{xx} = M_{xx}^{(1)} + M_{xx}^{(3)}, \quad M_{yy} = M_{yy}^{(1)} + M_{yy}^{(3)}, \quad M_{xy} = M_{xy}^{(1)} + M_{xy}^{(3)}.$$

Eq. (34) can be stated utilizing Eqs. (1), (19), (20), and (22) as

$$\begin{aligned}
N_{xx}^{(k)} &= A_{11}^{(k)} \frac{\partial u_k}{\partial x} + A_{12}^{(k)} \frac{\partial v_k}{\partial y} - B_{11}^{(k)} \frac{\partial^2 w}{\partial x^2} - B_{12}^{(k)} \frac{\partial^2 w}{\partial y^2}, \\
N_{yy}^{(k)} &= A_{12}^{(k)} \frac{\partial u_k}{\partial x} + A_{22}^{(k)} \frac{\partial v_k}{\partial y} - B_{12}^{(k)} \frac{\partial^2 w}{\partial x^2} - B_{22}^{(k)} \frac{\partial^2 w}{\partial y^2}, \\
N_{xy}^{(k)} &= A_{66}^{(k)} \frac{\partial u_k}{\partial y} + A_{66}^{(k)} \frac{\partial v_k}{\partial x} - 2B_{66}^{(k)} \frac{\partial^2 w}{\partial x \partial y}, \\
\\
M_{xx} &= B_{11}^{(1)} \frac{\partial u_1}{\partial x} + B_{11}^{(3)} \frac{\partial u_3}{\partial x} + B_{12}^{(1)} \frac{\partial v_1}{\partial y} + B_{12}^{(3)} \frac{\partial v_3}{\partial y} - (D_{11}^{(1)} + D_{11}^{(3)}) \frac{\partial^2 w}{\partial x^2} - (D_{12}^{(1)} + D_{12}^{(3)}) \frac{\partial^2 w}{\partial y^2}, \\
M_{yy} &= B_{12}^{(1)} \frac{\partial u_1}{\partial x} + B_{12}^{(3)} \frac{\partial u_3}{\partial x} + B_{22}^{(1)} \frac{\partial v_1}{\partial y} + B_{22}^{(3)} \frac{\partial v_3}{\partial y} - (D_{12}^{(1)} + D_{12}^{(3)}) \frac{\partial^2 w}{\partial x^2} - (D_{22}^{(1)} + D_{22}^{(3)}) \frac{\partial^2 w}{\partial y^2}, \\
M_{xy} &= B_{66}^{(1)} \frac{\partial u_1}{\partial y} + B_{66}^{(3)} \frac{\partial u_3}{\partial y} + B_{66}^{(1)} \frac{\partial v_1}{\partial x} + B_{66}^{(3)} \frac{\partial v_3}{\partial x} - 2(D_{66}^{(1)} + D_{66}^{(3)}) \frac{\partial^2 w}{\partial x \partial y}, \\
\\
Q_{xz}^{(2)} &= G_2^* \left( u_3 - u_1 + h_2 d \frac{\partial w}{\partial x} \right), \quad Q_{yz}^{(2)} = G_2^* \left( v_3 - v_1 + h_2 d \frac{\partial w}{\partial y} \right),
\end{aligned} \tag{35}$$

where

$$\begin{Bmatrix} A_{ij}^{(k)} \\ B_{ij}^{(k)} \\ D_{ij}^{(k)} \end{Bmatrix} = \int_{-\frac{h_k}{2}}^{\frac{h_k}{2}} Q_{ij}^{(k)} \begin{Bmatrix} 1 \\ z_k \\ z_k^2 \end{Bmatrix} dz_k. \tag{36}$$

The virtual work done by the external non-conservative loads can be presented as follows:

$$\delta W_{n.c.} = \iint_S q_f \delta w dS, \tag{37}$$

in which  $q_f$  is the distributed load per unit area applied by the foundation which can be presented based on the visco-Pasternak foundation model as

$$q_f = -k_w w - c \frac{\partial w}{\partial t} + k_p \left( \frac{\partial^2 w}{\partial x^2} + \frac{\partial^2 w}{\partial y^2} \right), \tag{38}$$

where  $k_w$ ,  $k_p$ , and  $c$  represent Winkler, Pasternak, and damping coefficients of the foundation, respectively. Substituting Eqs. (28), (33), and (37) into Eq. (24) leads to the following set of governing equations:

$$\begin{aligned}
\delta u_1: \frac{\partial N_{xx}^{(1)}}{\partial x} + \frac{\partial N_{xy}^{(1)}}{\partial y} + \frac{Q_{xz}^{(2)}}{h_2} - J_0^{(1)} \frac{\partial^2 u_1}{\partial t^2} - J_0^{(2)} \frac{\partial^2 u_3}{\partial t^2} + J_1^{(1)} \frac{\partial^3 w}{\partial t^2 \partial x} &= 0, \\
\delta u_3: \frac{\partial N_{xx}^{(3)}}{\partial x} + \frac{\partial N_{xy}^{(3)}}{\partial y} - \frac{Q_{xz}^{(2)}}{h_2} - J_0^{(2)} \frac{\partial^2 u_1}{\partial t^2} - J_0^{(3)} \frac{\partial^2 u_3}{\partial t^2} + J_1^{(3)} \frac{\partial^3 w}{\partial t^2 \partial x} &= 0, \\
\delta v_1: \frac{\partial N_{yy}^{(1)}}{\partial y} + \frac{\partial N_{xy}^{(1)}}{\partial x} + \frac{Q_{yz}^{(2)}}{h_2} - J_0^{(1)} \frac{\partial^2 v_1}{\partial t^2} - J_0^{(2)} \frac{\partial^2 v_3}{\partial t^2} + J_1^{(1)} \frac{\partial^3 w}{\partial t^2 \partial y} &= 0, \\
\delta v_3: \frac{\partial N_{yy}^{(3)}}{\partial y} + \frac{\partial N_{xy}^{(3)}}{\partial x} - \frac{Q_{yz}^{(2)}}{h_2} - J_0^{(2)} \frac{\partial^2 v_1}{\partial t^2} - J_0^{(3)} \frac{\partial^2 v_3}{\partial t^2} + J_1^{(3)} \frac{\partial^3 w}{\partial t^2 \partial y} &= 0, \\
\delta w: \frac{\partial^2 M_{xx}}{\partial x^2} + \frac{\partial^2 M_{yy}}{\partial y^2} + 2 \frac{\partial^2 M_{xy}}{\partial x \partial y} + d \frac{\partial Q_{xz}^{(2)}}{\partial x} + d \frac{\partial Q_{yz}^{(2)}}{\partial y} + q_f - J_1^{(1)} \frac{\partial^3 u_1}{\partial t^2 \partial x} \\
- J_1^{(3)} \frac{\partial^3 u_3}{\partial t^2 \partial x} - J_1^{(1)} \frac{\partial^2 v_1}{\partial t^2 \partial y} - J_1^{(3)} \frac{\partial^2 v_3}{\partial t^2 \partial y} + J_2 \frac{\partial^3 w}{\partial t^2 \partial x^2} + J_2 \frac{\partial^3 w}{\partial t^2 \partial y^2} - I_0 \frac{\partial^2 w}{\partial t^2} &= 0,
\end{aligned} \tag{39}$$

in which

$$\begin{aligned}
J_0^{(1)} &= I_0^{(1)} + \frac{I_0^{(2)}}{4} + \frac{I_2^{(2)}}{h_2^2}, \quad J_1^{(1)} = \frac{h_f}{h_2^2} I_2^{(2)}, \quad J_0^{(2)} = \frac{I_0^{(2)}}{4} - \frac{I_2^{(2)}}{h_2^2}, \\
J_0^{(3)} &= I_0^{(3)} + \frac{I_0^{(2)}}{4} + \frac{I_2^{(2)}}{h_2^2}, \quad J_1^{(3)} = -\frac{h_f}{h_2^2} I_2^{(2)}, \quad J_2 = I_2^{(1)} + I_2^{(3)} + \frac{I_2^{(2)} h_f^2}{h_2^2}.
\end{aligned} \tag{40}$$

Substituting Eqs. (35) and (38) into Eq. (39) leads to the following set of governing equations:

$$\begin{aligned}
A_{11}^{(1)} \frac{\partial^2 u_1}{\partial x^2} + A_{66}^{(1)} \frac{\partial^2 u_1}{\partial y^2} - \frac{G_2^*}{h_2} u_1 + \frac{G_2^*}{h_2} u_3 + (A_{12}^{(1)} + A_{66}^{(1)}) \frac{\partial^2 v_1}{\partial x \partial y} - B_{11}^{(1)} \frac{\partial^3 w}{\partial x^3} \\
- (B_{12}^{(1)} + 2B_{66}^{(1)}) \frac{\partial^3 w}{\partial x \partial y^2} + G_2^* d \frac{\partial w}{\partial x} - J_0^{(1)} \frac{\partial^2 u_1}{\partial t^2} - J_0^{(2)} \frac{\partial^2 u_3}{\partial t^2} + J_1^{(1)} \frac{\partial^3 w}{\partial t^2 \partial x} &= 0, \\
\frac{G_2^*}{h_2} u_1 + A_{11}^{(3)} \frac{\partial^2 u_3}{\partial x^2} + A_{66}^{(3)} \frac{\partial^2 u_3}{\partial y^2} - \frac{G_2^*}{h_2} u_3 + (A_{12}^{(3)} + A_{66}^{(3)}) \frac{\partial^2 v_3}{\partial x \partial y} - B_{11}^{(3)} \frac{\partial^3 w}{\partial x^3} \\
- (B_{12}^{(3)} + 2B_{66}^{(3)}) \frac{\partial^3 w}{\partial x \partial y^2} - G_2^* d \frac{\partial w}{\partial x} - J_0^{(2)} \frac{\partial^2 u_1}{\partial t^2} - J_0^{(3)} \frac{\partial^2 u_3}{\partial t^2} + J_1^{(3)} \frac{\partial^3 w}{\partial t^2 \partial x} &= 0, \\
(A_{12}^{(1)} + A_{66}^{(1)}) \frac{\partial^2 u_1}{\partial x \partial y} + A_{66}^{(1)} \frac{\partial^2 v_1}{\partial x^2} + A_{22}^{(1)} \frac{\partial^2 v_1}{\partial y^2} - \frac{G_2^*}{h_2} v_1 + \frac{G_2^*}{h_2} v_3 - (B_{12}^{(1)} + 2B_{66}^{(1)}) \frac{\partial^3 w}{\partial x^2 \partial y} \\
- B_{22}^{(1)} \frac{\partial^3 w}{\partial y^3} + G_2^* d \frac{\partial w}{\partial y} - J_0^{(1)} \frac{\partial^2 v_1}{\partial t^2} - J_0^{(2)} \frac{\partial^2 v_3}{\partial t^2} + J_1^{(1)} \frac{\partial^3 w}{\partial t^2 \partial y} &= 0, \\
(A_{12}^{(3)} + A_{66}^{(3)}) \frac{\partial^2 u_3}{\partial x \partial y} + \frac{G_2^*}{h_2} v_1 + A_{66}^{(3)} \frac{\partial^2 v_3}{\partial x^2} + A_{22}^{(3)} \frac{\partial^2 v_3}{\partial y^2} - \frac{G_2^*}{h_2} v_3 - (B_{12}^{(3)} + 2B_{66}^{(3)}) \frac{\partial^3 w}{\partial x^2 \partial y} \\
- B_{22}^{(3)} \frac{\partial^3 w}{\partial y^3} - G_2^* d \frac{\partial w}{\partial y} - J_0^{(2)} \frac{\partial^2 v_1}{\partial t^2} - J_0^{(3)} \frac{\partial^2 v_3}{\partial t^2} + J_1^{(3)} \frac{\partial^3 w}{\partial t^2 \partial y} &= 0,
\end{aligned} \tag{41}$$

$$\begin{aligned}
& B_{11}^{(1)} \frac{\partial^3 u_1}{\partial x^3} + \left( B_{12}^{(1)} + 2B_{66}^{(1)} \right) \frac{\partial^3 u_1}{\partial x \partial y^2} - G_2^* d \frac{\partial u_1}{\partial x} + B_{11}^{(3)} \frac{\partial^3 u_3}{\partial x^3} + \left( B_{12}^{(3)} + 2B_{66}^{(3)} \right) \frac{\partial^3 u_3}{\partial x \partial y^2} + G_2^* d \frac{\partial u_3}{\partial x} \\
& + \left( B_{12}^{(1)} + 2B_{66}^{(1)} \right) \frac{\partial^3 v_1}{\partial x^2 \partial y} + B_{22}^{(1)} \frac{\partial^3 v_1}{\partial y^3} - G_2^* d \frac{\partial v_1}{\partial y} + \left( B_{12}^{(3)} + 2B_{66}^{(3)} \right) \frac{\partial^3 v_3}{\partial x^2 \partial y} + B_{22}^{(3)} \frac{\partial^3 v_3}{\partial y^3} + G_2^* d \frac{\partial v_3}{\partial y} \\
& - \left( D_{11}^{(1)} + D_{11}^{(3)} \right) \frac{\partial^4 w}{\partial x^4} - 2 \left[ D_{12}^{(1)} + D_{12}^{(3)} + 2 \left( D_{66}^{(1)} + D_{66}^{(3)} \right) \right] \frac{\partial^4 w}{\partial x^2 \partial y^2} + \left( G_2^* h_2 d^2 + k_p \right) \frac{\partial^2 w}{\partial x^2} \\
& - \left( D_{22}^{(1)} + D_{22}^{(3)} \right) \frac{\partial^4 w}{\partial y^4} + \left( G_2^* h_2 d^2 + k_p \right) \frac{\partial^2 w}{\partial y^2} - k_w w - c \frac{\partial w}{\partial t} - J_1^{(1)} \frac{\partial^3 u_1}{\partial t^2 \partial x} - J_1^{(3)} \frac{\partial^3 u_3}{\partial t^2 \partial x} \\
& - J_1^{(1)} \frac{\partial^2 v_1}{\partial t^2 \partial y} - J_1^{(3)} \frac{\partial^2 v_3}{\partial t^2 \partial y} + J_2 \frac{\partial^3 w}{\partial t^2 \partial x^2} + J_2 \frac{\partial^3 w}{\partial t^2 \partial y^2} - I_0 \frac{\partial^2 w}{\partial t^2} = 0.
\end{aligned}$$

### 3 SOLUTION PROCEDURE

Utilizing Navier's method, the displacement field can be considered for a simply supported plate as follows:

$$\begin{aligned}
u_k(x, y, t) &= \sum_{m=1}^{\infty} \sum_{n=1}^{\infty} U_{mn}^{(k)} \exp(i\omega_{mn} t) \cos(\alpha x) \sin(\beta y) \\
v_k(x, y, t) &= \sum_{m=1}^{\infty} \sum_{n=1}^{\infty} V_{mn}^{(k)} \exp(i\omega_{mn} t) \sin(\alpha x) \cos(\beta y) \\
w(x, y, t) &= \sum_{m=1}^{\infty} \sum_{n=1}^{\infty} W_{mn} \exp(i\omega_{mn} t) \sin(\alpha x) \sin(\beta y)
\end{aligned} \tag{42}$$

in which  $\omega_{mn}$  is a complex eigenvalue and

$$\alpha = \frac{m\pi}{a}, \quad \beta = \frac{n\pi}{b}. \tag{43}$$

Substituting Eq. (42) into Eq. (41) leads to the following eigenvalue equation:

$$\left( [K] + \omega_{mn} [C] + \omega_{mn}^2 [M] \right) \{r\} = \{0\} \tag{44}$$

where

$$\{r\} = \begin{Bmatrix} U_{mn}^{(1)} \\ U_{mn}^{(3)} \\ V_{mn}^{(1)} \\ V_{mn}^{(3)} \\ W_{mn} \end{Bmatrix}, \quad [C] = -ic \begin{bmatrix} 0 & 0 & 0 & 0 & 0 \\ 0 & 0 & 0 & 0 & 0 \\ 0 & 0 & 0 & 0 & 0 \\ 0 & 0 & 0 & 0 & 0 \\ 0 & 0 & 0 & 0 & 1 \end{bmatrix}, \quad [K] = \begin{bmatrix} K_{11} & K_{12} & K_{13} & 0 & K_{15} \\ K_{21} & K_{22} & 0 & K_{24} & K_{25} \\ K_{31} & 0 & K_{33} & K_{34} & K_{35} \\ 0 & K_{42} & K_{43} & K_{44} & K_{45} \\ K_{51} & K_{52} & K_{53} & K_{54} & K_{55} \end{bmatrix}, \tag{45}$$

$$[M] = \begin{bmatrix} J_0^{(1)} & J_0^{(2)} & 0 & 0 & -\alpha J_1^{(1)} \\ J_0^{(2)} & J_0^{(3)} & 0 & 0 & -\alpha J_1^{(3)} \\ 0 & 0 & J_0^{(1)} & J_0^{(2)} & -\beta J_1^{(1)} \\ 0 & 0 & J_0^{(2)} & J_0^{(3)} & -\beta J_1^{(3)} \\ -\alpha J_1^{(1)} & -\alpha J_1^{(3)} & -\beta J_1^{(1)} & -\beta J_1^{(3)} & (\alpha^2 + \beta^2) J_2 + I_0 \end{bmatrix},$$

$$\begin{aligned}
K_{11} &= -\left(\alpha^2 A_{11}^{(1)} + \beta^2 A_{66}^{(1)} + \frac{G_2^*}{h_2}\right), \quad K_{12} = \frac{G_2^*}{h_2}, \quad K_{13} = -\alpha\beta(A_{12}^{(1)} + A_{66}^{(1)}), \\
K_{15} &= \alpha^3 B_{11}^{(1)} + \alpha\beta^2(B_{12}^{(1)} + 2B_{66}^{(1)}) + \alpha d G_2^*, \quad K_{22} = -\left(\alpha^2 A_{11}^{(3)} + \beta^2 A_{66}^{(3)} + \frac{G_2^*}{h_2}\right), \\
K_{24} &= -\alpha\beta(A_{12}^{(3)} + A_{66}^{(3)}), \quad K_{25} = \alpha^3 B_{11}^{(3)} + \alpha\beta^2(B_{12}^{(3)} + 2B_{66}^{(3)}) - \alpha d G_2^*, \\
K_{33} &= -\left(\alpha^2 A_{66}^{(1)} + \beta^2 A_{22}^{(1)} + \frac{G_2^*}{h_2}\right), \quad K_{34} = \frac{G_2^*}{h_2}, \\
K_{35} &= \alpha^2\beta(B_{12}^{(1)} + 2B_{66}^{(1)}) + \beta^3 B_{22}^{(1)} + \beta d G_2^*, \quad K_{44} = -\left(\alpha^2 A_{66}^{(3)} + \beta^2 A_{22}^{(3)} + \frac{G_2^*}{h_2}\right), \\
K_{45} &= \alpha^2\beta(B_{12}^{(3)} + 2B_{66}^{(3)}) + \beta^3 B_{22}^{(3)} - \beta d G_2^*, \\
K_{55} &= -\left\{\alpha^4(D_{11}^{(1)} + D_{11}^{(3)}) + 2\alpha^2\beta^2[D_{12}^{(1)} + D_{12}^{(3)} + 2(D_{66}^{(1)} + D_{66}^{(3)})]\right. \\
&\quad \left.+ (\alpha^2 + \beta^2)(G_2^* h_2 d^2 + k_p) + \beta^4(D_{22}^{(1)} + D_{22}^{(3)}) + k_w\right\},
\end{aligned}$$

The solution of the eigenvalue equation (44) provides the complex eigenvalues of the plate ( $\omega_{mn}$ ). Using the following relations, the natural frequencies ( $\Omega_{mn}$ ) and the corresponding loss factor ( $\eta_{mn}$ ) can be obtained [37]:

$$\Omega_{mn} = \sqrt{\operatorname{Re}(\omega_{mn}^2)}, \quad \eta_{mn} = \frac{\operatorname{Im}(\omega_{mn}^2)}{\operatorname{Re}(\omega_{mn}^2)}. \quad (46)$$

The loss factor is a dimensionless parameter and the dimensionless definition of the natural frequency is defined as follows:

$$\lambda_{mn} = \Omega_{mn} a \sqrt{\frac{\rho_m}{E_m}}. \quad (47)$$

#### 4 NUMERICAL RESULTS

In the current section, numerical results are provided for the presented model. Except for the cases which are mentioned directly, a sandwich rectangular plate of  $a=1$  m,  $b/a=2$ ,  $h/a=0.05$ , and  $h_2/h=0.6$  is considered. The face sheets are made of epoxy as the matrix enriched with GPLs and reinforced with glass fibers (see Table 2). Total mass fractions of the GPLs and glass fibers in the face sheets respectively are considered as  $W_{GPL}=0.01$  (1 %) and  $W_f=0.6$  (60 %) and fibers are oriented in both bottom and top face sheets as  $\varphi=[0/90^\circ/0/90^\circ]$ . The density of the core is  $2384.2$  kg/m<sup>3</sup>, the mass fraction of the CNTs in the MRE core is selected as  $W_{CNT}=1$  % and the magnetic field intensity is considered as  $B=500$  Gauss. Also, with the following definitions, the coefficients of the foundation are considered in a dimensionless form as  $k_w^*=0.01$ ,  $k_p^*=0.0001$ , and  $c^*=0.01$ :

$$k_w^* = \frac{k_w a}{E_m}, \quad k_p^* = \frac{k_p}{E_m a}, \quad c^* = \frac{c}{\sqrt{\rho_m E_m}}. \quad (48)$$

**Table 2**  
The mechanical properties of epoxy, GPLs, and glass fibers [34, 38]

| Epoxy                           | Glass fibers                        | GPLs                                |
|---------------------------------|-------------------------------------|-------------------------------------|
| $E_m=3$ GPa                     | $E_{11}^f=E_{22}^f=73.084$ GPa      | $E_{GPL}=1010$ GPa                  |
| $\nu_m=0.34$                    | $G_{12}^f=30.130$ GPa               | $\nu_{GPL}=0.186$                   |
| $\rho_m=1200$ kg/m <sup>3</sup> | $\nu_{12}^f=0.22$                   | $\rho_{GPL}=1060$ kg/m <sup>3</sup> |
|                                 | $\rho_f=2491.191$ kg/m <sup>3</sup> | $l_{GPL}=2.5$ $\mu$ m               |
|                                 |                                     | $w_{GPL}=1.5$ $\mu$ m               |
|                                 |                                     | $h_{GPL}=1.5$ nm                    |

As there is no available data for the natural frequencies and loss factors of the structure investigated in this paper, the verification is examined for a simpler case study. Consider a rectangular sandwich plate of  $a=0.3048$  m and  $b=0.3480$  m with homogenous isotropic face sheets of  $E_f=68.9$  GPa,  $\nu_f=0.3$ , and  $\rho_f=2740$  kg/m<sup>3</sup>, and  $h_f=0.762$  mm and a viscoelastic core of  $h_2=0.254$  mm. The complex shear modulus and density of the core respectively are selected as  $G_2^*=0.896(1+0.5i)$  MPa and  $\rho_2=999$  kg/m<sup>3</sup>. For various vibrational modes, values of the natural frequencies and corresponding loss factors are tabulated in Table 3 along with the corresponding ones reported by Johnson and Kienholz [39] and Cupial and Niziol [40]. As observed, results are in high agreement which approves the accuracy of the presented paper.

**Table 3**  
Natural frequencies and loss factors for a rectangular sandwich plate with homogenous isotropic face sheets and a viscoelastic core

| $(m,n)$ | Present            |             | Johnson and Kienholz [39] |             | Cupial and Niziol [40] |             |
|---------|--------------------|-------------|---------------------------|-------------|------------------------|-------------|
|         | $\Omega_{mn}$ (Hz) | $\eta_{mn}$ | $\Omega_{mn}$ (Hz)        | $\eta_{mn}$ | $\Omega_{mn}$ (Hz)     | $\eta_{mn}$ |
| (1,1)   | 60.24              | 0.190       | 60.30                     | 0.190       | 60.20                  | 0.190       |
| (1,2)   | 115.3              | 0.203       | 115.4                     | 0.203       | 115.2                  | 0.203       |
| (2,1)   | 130.5              | 0.199       | 130.6                     | 0.199       | 130.2                  | 0.199       |
| (2,2)   | 178.5              | 0.181       | 178.7                     | 0.181       | 178.5                  | 0.181       |
| (1,3)   | 195.5              | 0.174       | 195.7                     | 0.174       | 195.4                  | 0.174       |

Fig. 4 is provided to examine the effect of magnetic field intensity on the natural frequencies and loss factors of the plate in various vibrational modes. As shown in this figure, by increasing the magnetic field intensity both natural frequencies and loss factors of the plate increase in all vibrational modes. This enhancement can be explained using Fig. 2. As shown in Fig. 2, the higher magnetic field intensity results in higher storage modulus and loss factor. Thus, as the magnetic field intensity the stiffness and damping of the plate increase which leads to an increase in the natural frequencies and loss factors. It should be noted that the effect of magnetic field intensity on the free damped vibrational characteristics of the plate is inconspicuous and to make it possible to show the variations, the following definitions are utilized:

$$\lambda_{mn}^* = \frac{\lambda_{mn}}{\lambda_{mn}|_{B=0}}, \quad \eta_{mn}^* = \frac{\eta_{mn}}{\eta_{mn}|_{B=0}}. \quad (49)$$

Fig. 4 reveals that the higher vibrational modes are more sensitive to the magnetic field intensity. But, by increasing the magnetic field intensity from zero to 500 Gauss, the maximum increases in the natural frequencies and loss factors for  $(m,n)=(2,2)$  are less than 1 %.

For various vibrational modes, the influences of the mass fraction of the CNTs in the MRE core on the natural frequencies and loss factors of the plate are investigated in Table 3. As this table shows, by adjoining the CNTs to the MRE core from  $W_{CNT}=0$  to  $W_{CNT}=1$  %, the natural frequencies and corresponding loss factors experience a small growth. This increase can be explained by high values of the elastic moduli of the CNTs in comparison with MRE. Table 4 reveals that by increasing the mass fraction of the CNTs from  $W_{CNT}=0$  to  $W_{CNT}=1$  %, the maximum enhancement in the natural frequencies and loss factors is less than 0.5 %.

As revealed by Fig. 3 and Table 4, the magnetic field intensity and mass fraction of the CNTs in the MRE core have no remarkable effects on the free damped vibrational characteristics of the plate. To explain these inconspicuous effects, it should be noticed that the CNT-reinforced core bears only the shear components of the stress tensor and it has no sensible effect on the flexural rigidity of the plate which plays the dominant role in the free vibrational characteristics of the plate.

**Table 4**  
Effects of mass fraction of the CNTs in the MRE core on the natural frequencies and loss factors

| $(m,n)$ | $\lambda_{mn}$ |                 |               | $\eta_{mn}$ |                 |               |
|---------|----------------|-----------------|---------------|-------------|-----------------|---------------|
|         | $W_{CNT}=0$    | $W_{CNT}=0.5\%$ | $W_{CNT}=1\%$ | $W_{CNT}=0$ | $W_{CNT}=0.5\%$ | $W_{CNT}=1\%$ |
| (1,1)   | 0.3543         | 0.3548          | 0.3550        | 0.3245      | 0.3246          | 0.3247        |
| (1,2)   | 0.3734         | 0.3741          | 0.3745        | 0.3086      | 0.3087          | 0.3088        |
| (2,1)   | 0.4432         | 0.4444          | 0.4451        | 0.2611      | 0.2615          | 0.2617        |
| (2,2)   | 0.4661         | 0.4675          | 0.4682        | 0.2486      | 0.2490          | 0.2493        |

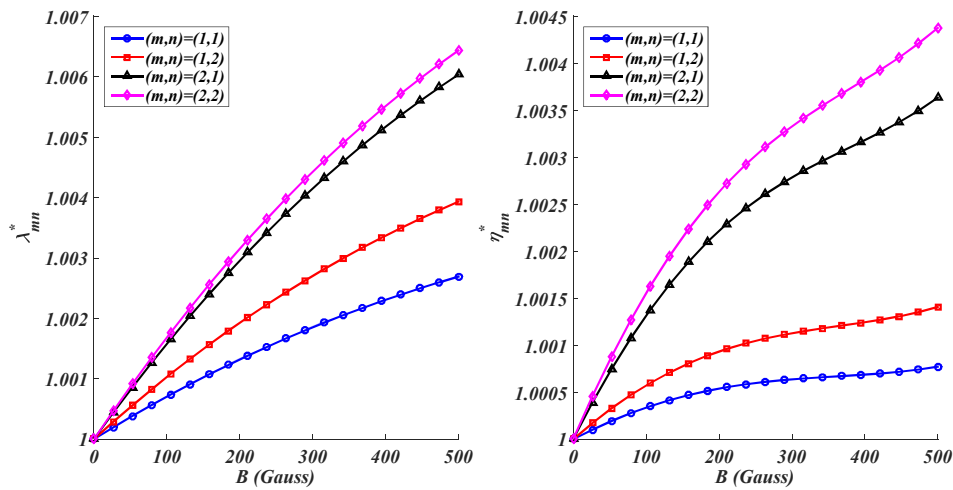


**Fig. 4**  
Effects of magnetic field intensity on the natural frequencies and loss factors.

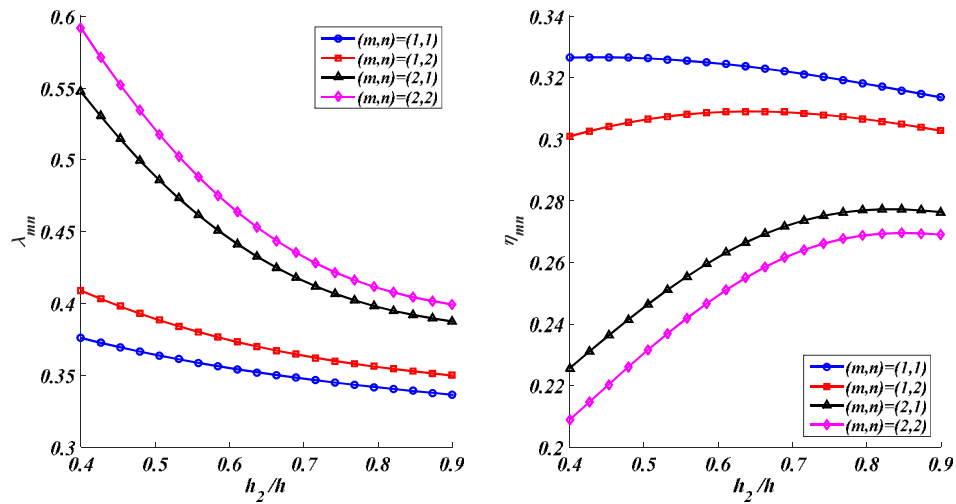


**Fig. 5**  
Effects of the thickness of CNT-reinforced MRE core on the natural frequencies and loss factors.

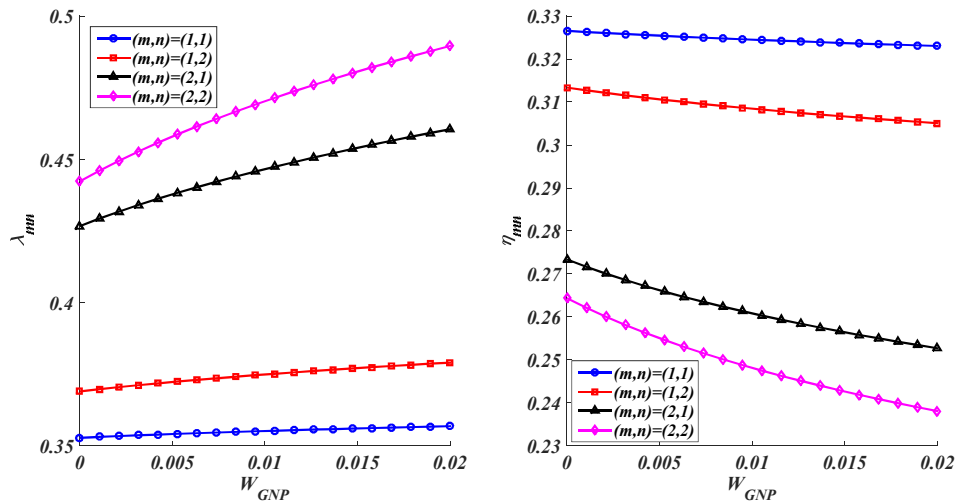


**Fig. 6**  
Effects of mass fraction of the GPLs in the face sheets on the natural frequencies and loss factors.

By considering a constant thickness for the plate, Fig. 5 shows the effects of the thickness of the CNT-reinforced MRE core on the natural frequencies and loss factors of the plate. This figure shows that as the thickness of the CNT-reinforced MRE core grows, the natural frequencies decrease in all vibrational modes and the corresponding loss factors experience an initial increase followed by a reduction. As the thickness of the CNT-reinforced MRE core increases, the thickness of the three-phase polymer/GPL/fiber face sheets decreases which reduces the flexural rigidity of the plate and leads to a considerable reduction in the natural frequencies. As Fig. 5 shows, for each vibrational mode, there is an optimum value of the thickness of the CNT-reinforced MRE core which provides the maximum damping. This optimum value can be affected by the mode numbers.

Fig. 6 is presented to study the influences of the mass fraction of the GPLs in the face sheets on the natural frequencies and loss factors of the plate. As observed, higher values of mass fraction of the GPLs in the face sheets result in higher natural frequencies and lower loss factors. As the GPLs benefit from a high value of the elastic modulus, subjoining more GPLs to the face sheets increases the flexural rigidity of the plate which increases the natural frequencies and reduces the loss factors in all vibrational modes.

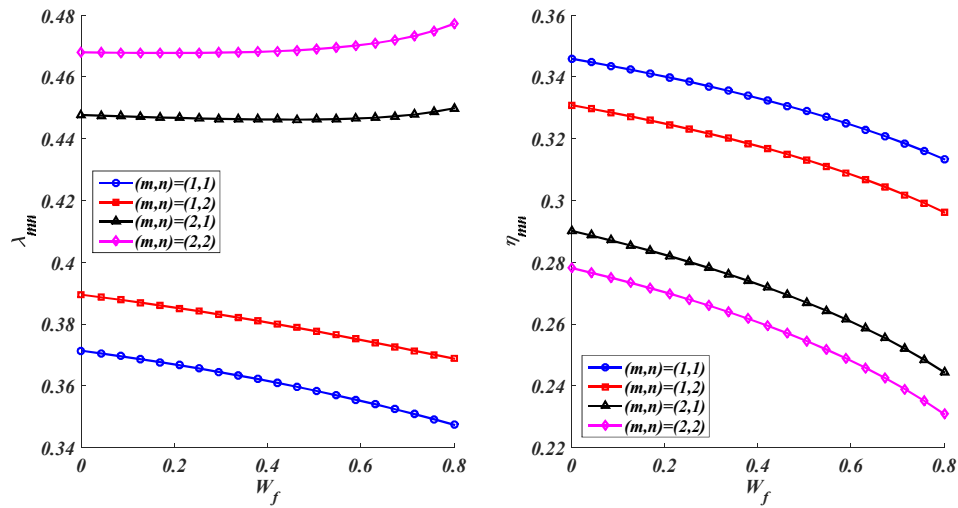


**Fig. 7** Effects of mass fraction of the glass fibers in the face sheets on the natural frequencies and loss factors.

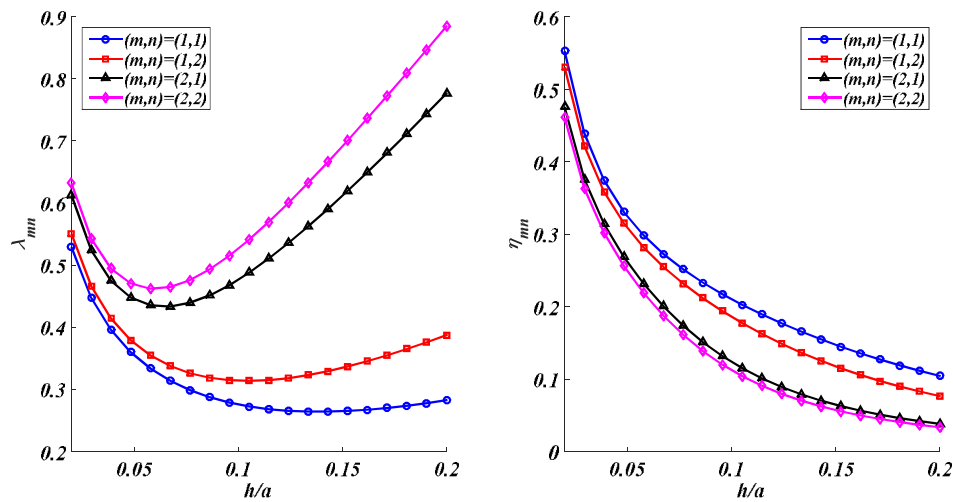


**Fig. 8** Effects of the thickness of the plate on the natural frequencies and loss factors.

The influences of the mass fraction of the glass fibers in the face sheets on the natural frequencies and loss factors of the plate are investigated in Fig. 7. This figure shows that as the mass fraction of the glass fibers increases, the loss factors decrease in all vibrational modes and no specific trend can be seen for the variation of the natural frequencies versus the variation of the mass fraction of the glass fibers. To explain this, it should be noted that based on Eq. (12), by increasing the mass fraction of the glass fibers, the mass fraction of the polymer and GPLs decrease, simultaneously. As Table 2 shows, the elastic moduli of the glass fibers are higher than the elastic modulus of the epoxy (matrix) and are smaller than the elastic modulus of the GPLs ( $E_m < E_{ij}^f < E_{GPL}$ ). Thus, depending on the vibration mode, an increase in the mass fraction of the glass fibers may result in either higher or lower stiffness and consequently higher or lower natural frequencies.

The effects of geometrical parameters of the plate on the sandwich plate such as thickness-to-length and aspect ratios. As the total thickness of the plate increases, both the stiffness and inertia of the plate grow. Consequently, as shown in Fig. 8, by increasing the thickness of the plate, the natural frequencies experience an initial drop followed by an increase. Fig. 8 reveals that by increasing the thickness of the plate the loss factors diminish in all vibrational modes which can be explained by an increase in the stiffness of the plate.

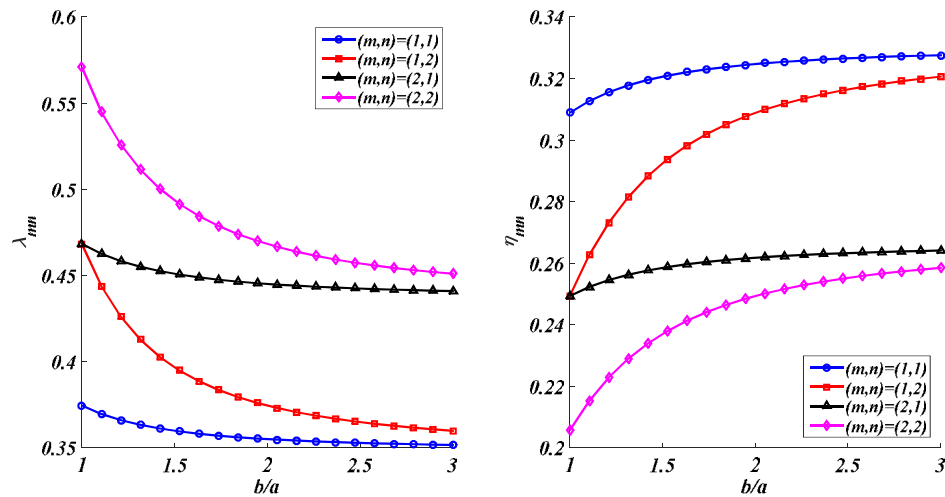


**Fig. 9**  
Effects of the length of the plate on the natural frequencies and loss factors.

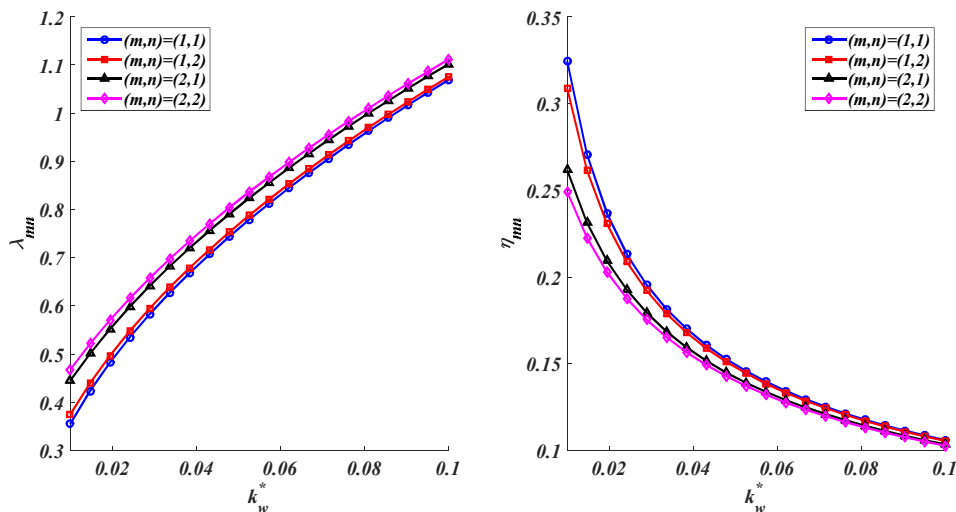


**Fig. 10**  
Effects of the Winkler coefficient of the foundation on the natural frequencies and loss factors.

An increase in the length of the plate reduces its stiffness and increases its inertia. Consequently, as Fig. 9 shows, by increasing the length of the plate, the natural frequencies decrease dramatically. Fig. 9 reveals that by increasing the length of the plate, the loss factors grow in all vibrational modes which can be explained by a reduction in the stiffness of the plate.

The influences of Winkler, Pasternak, and damping coefficients of the foundation on the natural frequencies and corresponding loss factors are examined in Figs. 10-12. An increase in the stiffness of the structure results in higher natural frequencies and a reduction in the damping of the structure [41]. Thus, as shown in Figs. 10 and 11, the natural frequencies grow and corresponding loss factors decrease by increasing the Winkler and Pasternak coefficients of the foundation which respectively show elastic and shear rigidity of the foundation.

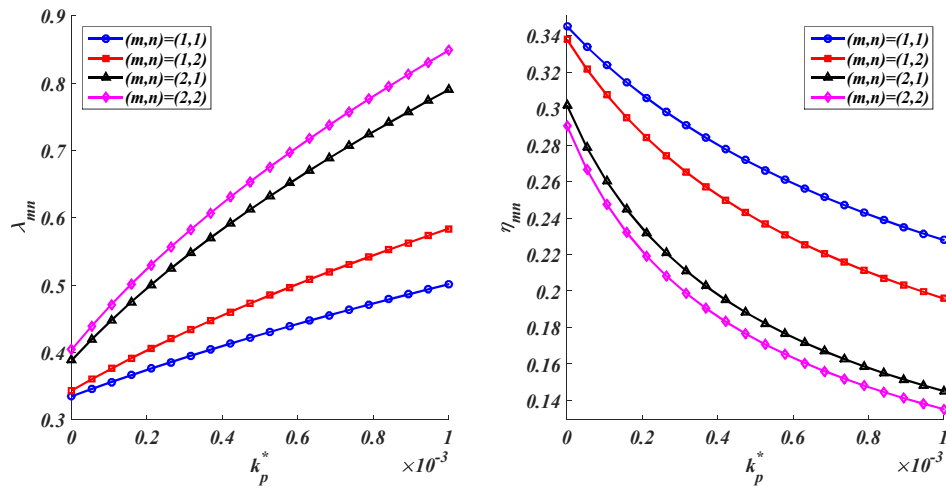


**Fig. 11**  
Effects of the Pasternak coefficient of the foundation on the natural frequencies and loss factors.

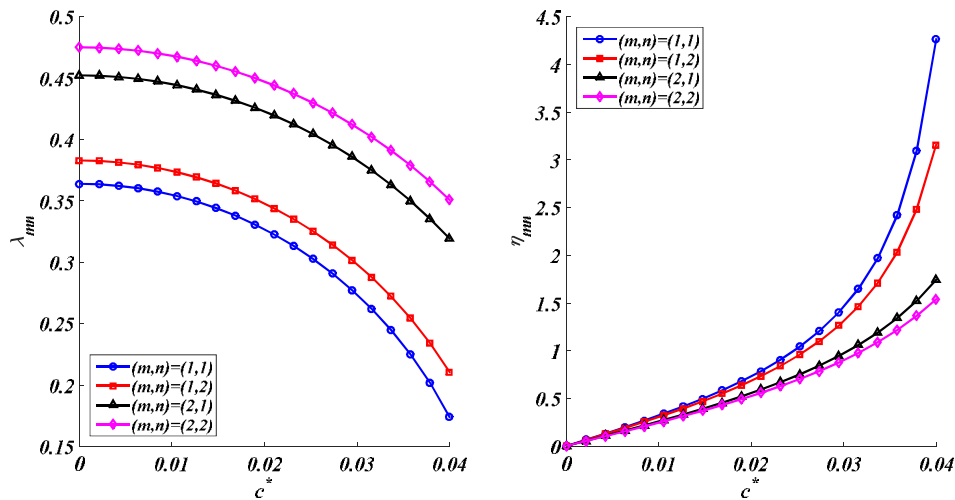


**Fig. 12**  
Effects of the damping coefficient of the foundation on the natural frequencies and loss factors.

An increase in the damping coefficients of the foundation leads to higher energy dissipation of the structure. Thus, as shown in Fig. 12, the natural frequencies decrease and corresponding loss factors increase by increasing the damping coefficients of the foundation.

## 5 CONCLUSIONS

In this paper, an exact solution was presented for the free damped vibration analysis of sandwich plates with CNT-reinforced MRE core and laminated three-phase polymer/GPL/fiber face sheets resting on a visco-Pasternak foundation. The main conclusions of this paper can be listed as follows:

- By increasing the magnetic field intensity, small enhancements can be seen in the natural frequencies of the plate and corresponding loss factors.

- The higher vibrational modes are more sensitive to the magnetic field intensity.
- Subjoining the CNTs to the MRE core leads to a small increase in the natural frequencies of the plate and corresponding loss factors.
  - By considering a specific thickness for the plate, by increasing the thickness of the CNT-reinforced MRE core, the natural frequencies decrease in all vibrational modes and the corresponding loss factors experience an initial growth followed by a reduction.
  - For each vibrational mode, there is an optimum value of the thickness of the CNT-reinforced MRE core which provides the highest damping.
  - As the mass fraction of the GPLs increases in the face sheets, the natural frequencies of the plate and corresponding loss factors grow.
  - As the mass fraction of the glass fibers increases, the loss factors decrease in all vibrational modes. But no specific trend can be seen for the variation of the natural frequencies versus the variation of the mass fraction of the glass fibers.
  - As the thickness of the plate grows, the natural frequencies experience an initial reduction followed by an increase.
  - As the length of the plate increases, the natural frequencies diminish dramatically and the corresponding loss factors increase in all vibrational modes.
  - As the Winkler (elastic) and Pasternak (shear) coefficients of the foundation increase, the natural frequencies grow and the corresponding loss factors decrease in all vibrational modes.
  - As the damping coefficient of the foundation increases, the natural frequencies diminish and the corresponding loss factors grow in all vibrational modes.

## REFERENCES

- [1] K. Rahmatnezhad, M. Zarastvand, R. Talebitooti, Mechanism study and power transmission feature of acoustically stimulated and thermally loaded composite shell structures with double curvature, *Composite Structures* 276 (2021) 114557.
- [2] M. Ghafouri, M. Ghassabi, M.R. Zarastvand, R. Talebitooti, Sound propagation of three-dimensional sandwich panels: influence of three-dimensional re-entrant auxetic core, *AIAA Journal* (2022) 1-11.
- [3] M. Zarastvand, M. Asadijafari, R. Talebitooti, Acoustic wave transmission characteristics of stiffened composite shell systems with double curvature, *Composite Structures* 292 (2022) 115688.
- [4] M. Zarastvand, M. Ghassabi, R. Talebitooti, Prediction of acoustic wave transmission features of the multilayered plate constructions: A review, *Journal of Sandwich Structures & Materials* 24(1) (2022) 218-293.
- [5] V. Lara-Prieto, R. Parkin, M. Jackson, V. Silberschmidt, Z. Keşy, Vibration characteristics of MR cantilever sandwich beams: experimental study, *Smart Materials and structures* 19(1) (2009) 015005.
- [6] B. Nayak, S. Dwivedy, K. Murthy, Dynamic analysis of magnetorheological elastomer-based sandwich beam with conductive skins under various boundary conditions, *Journal of Sound and Vibration* 330(9) (2011) 1837-1859.
- [7] B. Nayak, S. Dwivedy, K. Murthy, Dynamic stability of a rotating sandwich beam with magnetorheological elastomer core, *European Journal of Mechanics-A/Solids* 47 (2014) 143-155.
- [8] V. Rajamohan, V. Sundararaman, B. Govindarajan, Finite element vibration analysis of a magnetorheological fluid sandwich beam, *Procedia Engineering* 64 (2013) 603-612.
- [9] H. Navazi, S. Bornassi, H. Haddadpour, Vibration analysis of a rotating magnetorheological tapered sandwich beam, *International Journal of Mechanical Sciences* 122 (2017) 308-317.
- [10] M.R. Rohn-Abadi, P. Shahali, H. Haddadpour, Effects of magnetoelastic loads on free vibration characteristics of the magnetorheological-based sandwich beam, *Journal of Intelligent Material Systems and Structures* 31(7) (2020) 1015-1028.
- [11] A. Omid Soroor, M. Asgari, H. Haddadpour, Effect of axially graded constraining layer on the free vibration properties of three layered sandwich beams with magnetorheological fluid core, *Composite Structures* 255 (2021) 112899.
- [12] S. Aguib, A. Nour, H. Zahloul, G. Bossis, Y. Chevalier, P. Lançon, Dynamic behavior analysis of a magnetorheological elastomer sandwich plate, *International Journal of Mechanical Sciences* 87 (2014) 118-136.
- [13] G. Payganeh, K. Malekzadeh, H. Malek Mohammadi, Free vibration of sandwich panels with smart magneto-rheological layers and flexible cores, *Journal of Solid Mechanics* 8(1) (2016) 12-30.
- [14] J.-Y. Yeh, Vibration characteristics analysis of orthotropic rectangular sandwich plate with magnetorheological elastomer, *Procedia Engineering* 79 (2014) 378-385.
- [15] M. Eshaghi, The effect of magnetorheological fluid and aerodynamic damping on the flutter boundaries of MR fluid sandwich plates in supersonic airflow, *European Journal of Mechanics-A/Solids* 82 (2020) 103997.

- [16] S. Givi, A. Ghorbanpour Arani, Z. Khoddami Maraghi, E. Arshid, Free vibration and supersonic flutter analyses of a sandwich cylindrical shell with CNT-reinforced honeycomb core integrated with piezoelectric layers, *Mechanics Based Design of Structures and Machines* (2024) 1-29.
- [17] A. Ghorbanpour-Arani, Z. Khoddami Maraghi, A. Ghorbanpour Arani, The Frequency Response of Intelligent Composite Sandwich Plate Under Biaxial In-Plane Forces, *Journal of Solid Mechanics* 15 (1) (2023)1-18.
- [18] E. Haghparast, A. Ghorbanpour-Arani, A. Ghorbanpour Arani, Effect of Fluid–Structure Interaction on Vibration of Moving Sandwich Plate With Balsa Wood Core and Nanocomposite Face Sheets, *International Journal of Applied Mechanics* 12(7) (2020) 2050078.
- [19] E. Arshid, Z. Khoddami Maraghi, Ö. Civalek, Variable-thickness higher-order sandwich beams with FG cellular core and CNT-RC patches: vibrational analysis in thermal environment, *Archive of Applied Mechanics* 95(1) (2025) 1-24.
- [20] M. Pakize, Z. Khoddami Maraghi, M. Irani Rahaghi, S. Niknejad, A. Ghorbanpour Arani, Monotonous, symmetric, and nonsymmetric patterns of porous core in vibration study of nano-composite sandwich plate bonded by piezoelectric sheets, *Journal of Computational Applied Mechanics* 53(3) (2022) 444-477.
- [21] Z. Khoddami Maraghi, Flutter and divergence instability of nanocomposite sandwich plate with magnetostrictive face sheets, *Journal of Sound and Vibration* 457 (2019) 240-260.
- [22] R. Selvaraj, M. Ramamoorthy, Experimental and finite element vibration analysis of CNT reinforced MR elastomer sandwich beam, *Mechanics Based Design of Structures and Machines* (2020) 1-13.
- [23] R. Selvaraj, M. Ramamoorthy, Dynamic analysis of laminated composite sandwich beam containing carbon nanotubes reinforced magnetorheological elastomer, *Journal of Sandwich Structures & Materials* 23(5) (2021) 1784-1807.
- [24] A.B. Arumugam, M. Subramani, M. Dalakoti, P. Jindal, R. Selvaraj, E. Khalife, Dynamic characteristics of laminated composite CNT reinforced MRE cylindrical sandwich shells using HSDT, *Mechanics Based Design of Structures and Machines* (2021) 1-17.
- [25] R. Selvaraj, M. Ramamoorthy, A.B. Arumugam, Experimental and numerical studies on dynamic performance of the rotating composite sandwich panel with CNT reinforced MR elastomer core, *Composite Structures* 277 (2021) 114560.
- [26] R. Selvaraj, M. Subramani, M. Ramamoorthy, Vibration characteristics and optimal design of composite sandwich beam with partially configured hybrid MR-Elastomers, *Mechanics Based Design of Structures and Machines* (2021) 1-17.
- [27] A.H. Yousefi, P. Memarzadeh, H. Afshari, S.J. Hosseini, Agglomeration effects on free vibration characteristics of three-phase CNT/polymer/fiber laminated truncated conical shells, *Thin-Walled Structures* 157 (2020) 107077.
- [28] A.H. Yousefi, P. Memarzadeh, H. Afshari, S.J. Hosseini, Optimization of CNT/polymer/fiber laminated truncated conical panels for maximum fundamental frequency and minimum cost, *Mechanics Based Design of Structures and Machines* (2021) 1-23.
- [29] A.H. Yousefi, P. Memarzadeh, H. Afshari, S.J. Hosseini, Dynamic characteristics of truncated conical panels made of FRPs reinforced with agglomerated CNTs, *Structures*, Elsevier, 2021, pp. 4701-4717.
- [30] H. Afshari, N. Adab, Size-dependent buckling and vibration analyses of GNP reinforced microplates based on the quasi-3D sinusoidal shear deformation theory, *Mechanics Based Design of Structures and Machines* In Press (2020).
- [31] H. Afshari, Free vibration analysis of GNP-reinforced truncated conical shells with different boundary conditions, *Australian Journal of Mechanical Engineering* 20(5) (2022) 1363-1378.
- [32] H. Afshari, Effect of graphene nanoplatelet reinforcements on the dynamics of rotating truncated conical shells, *Journal of the Brazilian Society of Mechanical Sciences and Engineering* 42(10) (2020) 1-22.
- [33] J.H. Afdl, J. Kardos, The Halpin–Tsai equations: a review, *Polymer Engineering & Science* 16(5) (1976) 344-352.
- [34] Y. Jeawon, G. Drosopoulos, G. Foutsitzi, G. Stavroulakis, S. Adali, Optimization and analysis of frequencies of multi-scale graphene/fibre reinforced nanocomposite laminates with non-uniform distributions of reinforcements, *Engineering Structures* 228 (2021) 111525.
- [35] M.K. Nasution, R. Syah, D. Ramdan, H. Afshari, H. Amirabadi, M.M. Selim, A. Khan, M.L. Rahman, M.S. Sarjadi, C.-H. Su, Modeling and computational simulation for supersonic flutter prediction of polymer/GNP/fiber laminated composite joined conical-conical shells, *Arabian Journal of Chemistry* 15(1) (2022) 103460.
- [36] J.N. Reddy, *Energy principles and variational methods in applied mechanics*, John Wiley & Sons, Hoboken, New Jersey, 2017.
- [37] D. Rao, Frequency and loss factors of sandwich beams under various boundary conditions, *Journal of Mechanical Engineering Science* 20(5) (1978) 271-282.
- [38] F. Tornabene, M. Baccocchi, N. Fantuzzi, J. Reddy, Multiscale approach for three-phase CNT/polymer/fiber laminated nanocomposite structures, *Polymer composites* 40(S1) (2019) E102-E126.
- [39] C.D. Johnson, D.A. Kienholz, Finite element prediction of damping in structures with constrained viscoelastic layers, *AIAA journal* 20(9) (1982) 1284-1290.
- [40] P. Cupial, J. Niziol, Vibration and damping analysis of a three-layered composite plate with a viscoelastic mid-layer, *Journal of Sound and Vibration* 183(1) (1995) 99-114.
- [41] S.S. Rao, *Mechanical vibrations*, Addison Wesley Boston, MA1995.